Transformation and Tempering Behavior of the Heat-Affected Zone of 2.25Cr-1Mo Steel

The tempering response of the HAZ is found to be a strong function of base metal microstructure and carbon content

BY D. K. HODGSON, T. DAI, AND J. C. LIPPOLD

ABSTRACT

The heat-affected zone (HAZ) tempering response of multiple heats of forged 2.25Cr-1Mo steel (F22) has been studied under conditions approximating welded corrosion-resistant cladding and using thermal simulation. A Hollomon-Jaffe tempering parameter was used to determine the effect of tempering temperature in the range of 638° to 677°C (1180° to 1250°F) for times up to 11 hours. Austenization and tempering treatments were also performed in order to determine the response of the starting base metal microstructure. The as-quenched hardness of the base materials with high carbon levels (0.14–0.17 wt-%) were lower than predicted due to the incomplete dissolution of alloy carbides. The HAZ hardness of the weld cladding and the thermal simulations performed at a peak temperature of 1350°C (2462°F) were close to the predicted values due to the apparent dissolution of the base metal carbides. In general, tempering of selected heats with carbon levels exceeding 0.15 wt-% carbon was not capable of reducing HAZ hardness below 250 VHN. At tempering times exceeding approximately 5 hours, some secondary hardening was observed due to the precipitation of Mo_2C carbides.

KEYWORDS

• F22 Steel • 2.25Cr-1Mo Steel • Heat-Affected Zone • Tempering • Hardness

Introduction

F22 is a forged chromium and molybdenum low-alloy steel commonly used in subsea service in the oil and gas industry. A critical concern in these applications is the potential exposure to sour production fluid. In these service conditions, exposure to hydrogen sulfide (H_2S) can lead to failure by sulfide stress corrosion cracking (SSC). While H_2S does not directly cause SSC failures, it contributes by increasing the relative amount of hydrogen absorption in low-alloy steels (Ref. 1). One common method to prevent this type of failure is to deposit a corrosion-resistant alloy cladding on surfaces that will be potentially exposed to production fluid using an arc welding process. Because SSC failure occurs due to a hydrogen embrittlement mechanism, the material hardness in the heat-affected zone (HAZ) resulting from the cladding process plays a critical role in the susceptibility to failure (Ref. 2). The National Society of Corrosion Engineers (NACE) and the International Organization for Standardization (ISO) has established guidelines in NACE MR0175/ ISO15156 that require the maximum hardness of the HAZ not exceed 22 HRC (or 250 VHN in certain situations).

In application, material heats of similar composition have shown differing results in HAZ hardness after postweld heat treatment (PWHT). Unpublished research conducted by Lippold and Fusner in 2010 verified this when studying two compositionally similar heats, which yielded different as-quenched hardness, tempered hardness, and tempering rates after identical solution austenization treatments (Ref. 3). This difference in tempering behavior can present a challenge in selecting appropriate PWHT. When longer and higher temperature austenization cycles were used, the quenched hardness of the two heats began to converge suggesting that the austenization temperature had an effect on the amount of free carbon available to produce the hardest quenched microstructure.

To further investigate this behavior, the study was expanded to include 15 additional heats plus one (L7976) included in the initial investigation. To understand the underlying cause of the variation in mechanical behavior after tempering and solution austenization treatments, several approaches were taken. First, base material samples were used for three different austenization treatments with the goal of achieving a homogeneous solutionized microstructure as indicated by the macrohardness in the as-quenched condition. Also, to investigate the tempering response of the HAZ, autogenous gas tungsten arc spot welds were produced and tempered through a range of tempering conditions as characterized by Holloman-Jaffe parameters. These samples were characterized by microhardness read-

D. K. HODGSON, T. DAI, and J. C. LIPPOLD are with The Ohio State University, Columbus, Ohio.

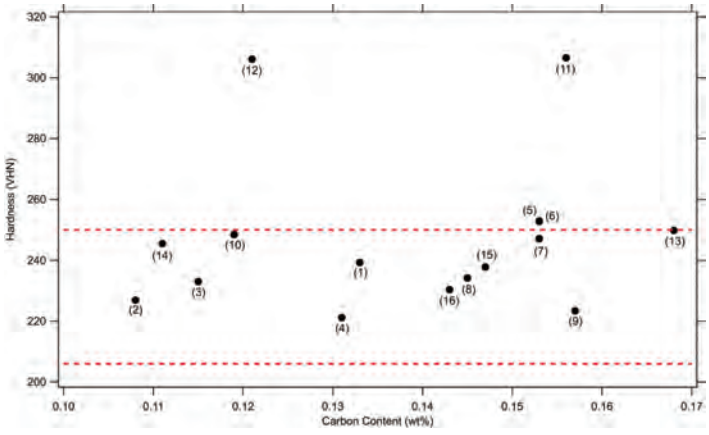

Fig. 1 — As-received base material hardness.

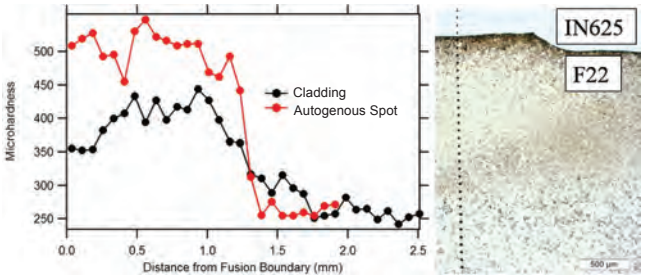

Fig. 2 — HAZ hardness traverses in a typical spot weld and IN625 cladding on F22 steel.

ings of the fusion zone and HAZ of each sample. Both the austenitized base material and spot welded samples were further characterized using light optical and scanning electron microscopy. In addition, Gleeble simulation of the coarse-grained heat-affected zone (CG-HAZ) was conducted on 4 of the 16 heats. The response of the samples to the Gleeble simulation was measured in the "as-welded" and tempered condition by microhardness measurements and microstructural evaluation, to compare the results with that of the autogenous spot weld samples.

Experimental Procedure

Materials. In order to expand on the preliminary study to a wider range of compositions, 16 heats of various forged product forms were provided by Cameron International. The compositions of these heats were determined by optical emission spectroscopy (OES) of the bulk material extracted from the forgings and are shown in Table 1. The carbon content ranged from 0.108 to 0.168 wt-%. The International Institute of Welding carbon equivalents (CE_{IIW}) ranged from 0.80 to 1.02 and P_{CM} values from 0.311 to 0.410. Material hardness is a critical factor used in the procurement of F22 with the result that most heats, regardless of composition, have approximately the same hardness as shown in Fig. 1. The horizontal lines shown indicate the typical acceptable range of hardness for forged and heat-treated F22. Note that virtually all of these heats have base metal hardness values at or below 250 VHN. Equation 1 shows the International Institute of Welding carbon equivalent equation and Equation 2 is the P_{CM} equation.

$$CE_{IIW} = C + \frac{Mn}{6} + \frac{CR + Mo + V}{5} + \frac{Ni + Cu}{15} \quad (1)$$

$$P_{CM} = C + \frac{Si}{30} + \frac{Mn + Cu + Cr}{20} + \frac{Ni}{60} + \frac{Mo}{15} + \frac{V}{10} + 5B \quad (2)$$

For solution austenization treatments, samples were sectioned into cubes 13 mm square (½ × ½ × ½ in.) and cleaned with ethyl alcohol to remove any cutting fluid residue. In order to prevent oxidation and decarburization during heat treatment, groups of five or six samples were encased in a quartz tube and sealed with 0.2 atmosphere partial pressure of argon. To investigate the response of these heats to welding, autogenous spot welds were produced on small base metal samples of dimension 10 × 19 × 19 mm (⅜ × ¾ × ¾ in.).

Solution austenization heat treatment. Samples were subjected to three different heat treatments, 954°C (1750°F) for 1 h, and 1148°C (2100°F) for 1 h and 4 h. These treatments were selected based on the requirements specified by ASTM A182 and thermodynamic simulations of the austenite phase field using JMatPro®. In each test, heat treatment time corresponds to total time in the furnace, including the heating time. During process development, sample temperature was found to reach the furnace set point temperature in approximately 5 min. Each tube was placed in a Lucifer model 7GT-K24 box furnace on a preheated nickel plate to facilitate fast removal. Once the heat treatment time was completed, the tubes were removed from the furnace and quenched in room temperature water. If the quartz tubes did not fracture due to the thermal shock, they were broken immediately to achieve the highest feasible cooling rate.

Spot welding procedure development. In order to simulate production welding conditions, autogenous gas tungsten arc spot welds made with various heat inputs were compared to a supplied sample that was clad in nickel Alloy 625 — Fig. 2. The base metal selected for procedural development was one with close chemical composition to that of the clad sample base material. Upon completion of welding, relative size and hardness distribution within the HAZs of each sample were compared. While the width of the HAZ is similar, the peak hardness in the cladding HAZ is lower, likely due to the tempering effect of the subsequent passes of the multilayer cladding. The parameters were selected that resulted in matching widths of the hardened region in the HAZ and are shown in Table 2. After completion of the welding cycle, the samples were allowed to free cool to room temperature.

Coarse-grained heat-affected zone simulations. A Gleeble™ thermomechanical simulator was used to generate simulated coarse-grain HAZ in Heats 2 (0.108 wt-% C), Heat 5 (0.153 wt-% C), Heat 10 (0.119 wt-% C), and Heat 13 (0.168 wt-% C). Round bar specimens with a gauge section diameter of 6.35 mm (0.25 in.) were heated at 100°C per second to a peak temperature

Table 1 — Composition of He ts of F22

Elem.	1	2	3	4	5	6	7	8	9	10	11	12	13	14	15	16	Min.	Max.	Mean	Std. Dev.
C	0.133	0.108	0.115	0.131	0.153	0.153	0.153	0.145	0.157	0.119	0.156	0.121	0.168	0.111	0.147	0.143	0.108	0.168	0.138	0.019
Cr	2.34	2.15	2.39	2.26	2.54	2.35	2.36	2.39	2.18	2.16	2.2	2.11	2.17	2.33	2.39	2.47	2.11	2.54	2.23	0.127
Mo	1.02	0.94	1.08	0.9	1.19	1.03	1.03	0.97	0.95	0.97	0.94	0.99	0.96	0.88	1.06	1.05	0.88	1.19	1.00	0.077
Mn	0.49	0.445	0.435	0.347	0.533	0.537	0.542	0.563	0.73	0.416	0.473	0.485	0.758	0.429	0.519	0.544	0.347	0.758	0.515	0.106
Si	0.34	0.2	0.292	0.228	0.203	0.29	0.29	0.239	0.135	0.158	0.227	0.24	0.188	0.441	0.281	0.308	0.135	0.441	0.253	0.075
Ni	0.134	0.025	0.123	0.15	0.28	0.08	0.08	0.148	0.24	0.19	0.08	0.033	0.302	0.22	0.208	0.171	0.025	0.302	0.154	0.083
Cu	0.159	0.02	0.234	0.124	0.19	0.089	0.091	0.097	0.187	0.204	0.146	0.03	0.194	0.145	0.071	0.087	0.02	0.234	0.129	0.063
Sn	0.009	0.002	0.012	0.008	0.012	0.007	0.008	0.008	0.009	0.018	0.01	0.003	0.009	0.012	0.008	0.009	0.002	0.018	0.009	0.004
Al	0.027	0.021	0.025	0.025	0.023	0.024	0.023	0.022	0.02	0.002	0.016	0.027	0.022	0.004	0.022	0.021	0.002	0.027	0.02	0.007
V	0.018	0.016	0.016	0.018	0.021	0.016	0.017	0.02	0.016	0.014	0.016	0.014	0.017	0.016	0.018	0.017	0.014	0.021	0.017	0.002
Nb	0.004	0.003	0.004	0.006	0.021	0.003	0.004	0.003	0.004	0.004	0.004	0.003	0.003	0.004	0.004	0.004	0.003	0.021	0.005	0.004
Zr	0.002	0.002	0.002	0.001	0.002	0.002	0.002	0.002	0.002	0.002	0.002	0.001	0.002	0.002	0.002	0.002	0.001	0.002	0.002	0.000
Ti	0.003	0.002	0.003	0.002	0.002	0.003	0.003	0.002	0.001	0.002	0.002	0.002	0.002	0.003	0.002	0.002	0.001	0.003	0.002	0.001
B	0.0002	0.0001	0.0002	0.0001	0.0001	0.0002	0.0002	0.0002	0.0003	0.0001	0.0002	0.0001	0.0004	0.0001	0.0001	0.0001	0.0001	0.0004	0.0002	0.0001
P	0.013	0.01	0.011	0.013	0.009	0.007	0.008	0.011	0.008	0.009	0.009	0.012	0.007	0.014	0.014	0.009	0.007	0.014	0.01	0.002
S	0.01	0.017	0.017	0.003	0.004	0.003	0.004	0.003	0.008	0.02	0.018	0.021	0.009	0.012	0.01	0.009	0.003	0.021	0.0105	0.006
Ca	0.0005	0.0002	0.0004	0.0003	0.0008	0.0003	0.0003	0.0001	0.006	0.0002	0.0007	0.0002	0.0059	0.0005	0.0003	0.002	0.0001	0.006	0.001	0.002
Co	0.011	0.004	0.013	0.015	0.025	0.01	0.01	0.011	0.014	0.016	0.01	0.004	0.019	0.015	0.014	0.015	0.004	0.025	0.013	0.005
IIWCE	0.909	0.807	0.909	0.842	1.023	0.933	0.937	0.932	0.937	0.843	0.882	0.829	0.957	0.853	0.945	0.958	0.807	1.023	0.906	0.058
P_{cm}	0.366	0.311	0.354	0.34	0.41	0.384	0.385	0.376	0.387	0.333	0.371	0.329	0.403	0.336	0.381	0.383	0.311	0.41	0.366	0.029

Table 2 — Parameters for Autogenous GTAW Spot Weld

Preheat Temperature	Ambient
Welding Current	100 A
Arc Length	2.54 mm
Voltage (approx.)	11.5–12 V
Hold Time	5 s
Shielding Gas	99.99% Ar

of 1350°C. The peak temperature was maintained for 1 s or 10 s before allowing the sample to free cool. The free cooling resulted in a Dt_{8-5} in the range from 7.5 to 9.5 s and was controlled by the free span between the two copper jaws of the Gleeble.

Tempering heat treatment. To determine the response of each heat to tempering heat treatments, samples were subjected to the seven tempering heat treatments shown in Table 3. These heat treatments were selected to represent Hollomon-Jaffe tempering parameters that span a postweld heat treatment procedure common in industrial production (HT-3 in Table 3). These values were calculated using Equation 3 with temperature (T) in kelvin and time (t) in hours (Ref. 4). During procedure development, thermocouple monitoring determined that samples reached furnace temperature in approximately 20 min. This heating time was not considered in the calculation of the Hollomon-Jaffe parameters. The furnace used was a horizontal Lindberg 59544 type. At the end of the tempering time, samples were quenched in room temperature water. (Equation 3 is the Holloman-Jaffe parameter (HJP) for tempering treatments).

$$HJP = T * (20 + LOG(t)) \qquad (3)$$

Hardness testing. The as-quenched hardness of each heat of material was measured on the Rockwell C scale using a Leco LR series hardness tester. Prior to indenting, the samples were sectioned through the centerline and another parallel plane in order to ensure a flat, parallel surface for accurate measurements. An average hardness was calculated based on four indents near the center of the cross section. Because of the smaller area, the simulated CGHAZ samples were measured with 100-g-load Vickers microhardness. Due to low hardness that prevented the use of the Rockwell C scale, the base material was measured with 1-kg Vickers microhardness indents ($VHN_{1.0}$). For each tempering treatment of each heat, a microhardness traverse from the fusion zone to the base material was used to measure the hardness as a function of the distance from the fusion boundary. Indents for these traverses were made with a 100-g load ($VHN_{0.1}$) and a spacing of 75 µm. These values were also used to calculate an average hardness of the HAZ for each tempering treatment.

Optical microscopy. After hardness testing, samples were mounted in Bakelite and ground using successive steps of 320-, 400-, and 600-grit wet silicon carbide abrasive papers and polished with 9-, 6-, 3-, and 1-µm diamond polishing paste. After a suitable surface was obtained, samples were chemically etched using Vilella's etch (5 cc HCL + 2 g picric acid + 100 cc ethyl alcohol) or 2/5% nital (2–5% nitric acid + ethyl alcohol) to increase contrast of microstructural features.

Results and Discussion

Hardness of as-quenched and simulated heats. The three separate solution austenization treatments were evaluated for each heat by comparing the hardness of the as-quenched microstructure. Because F22 transforms to mostly martensite during high cooling

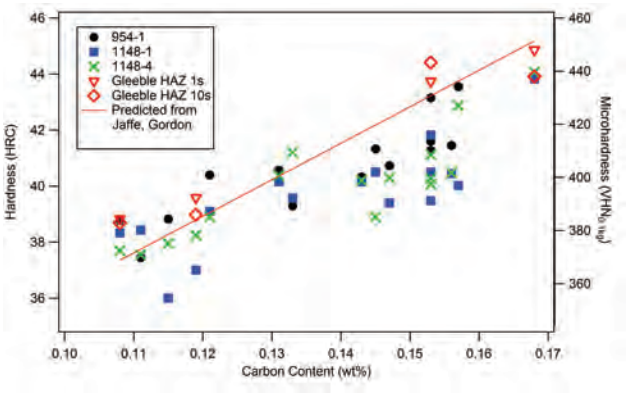

Fig. 3 — As-quenched and simulated coarse-grain heat-affected zone hardness as a function of carbon content as compared to the Jaffe and Gordon prediction (Ref. 6).

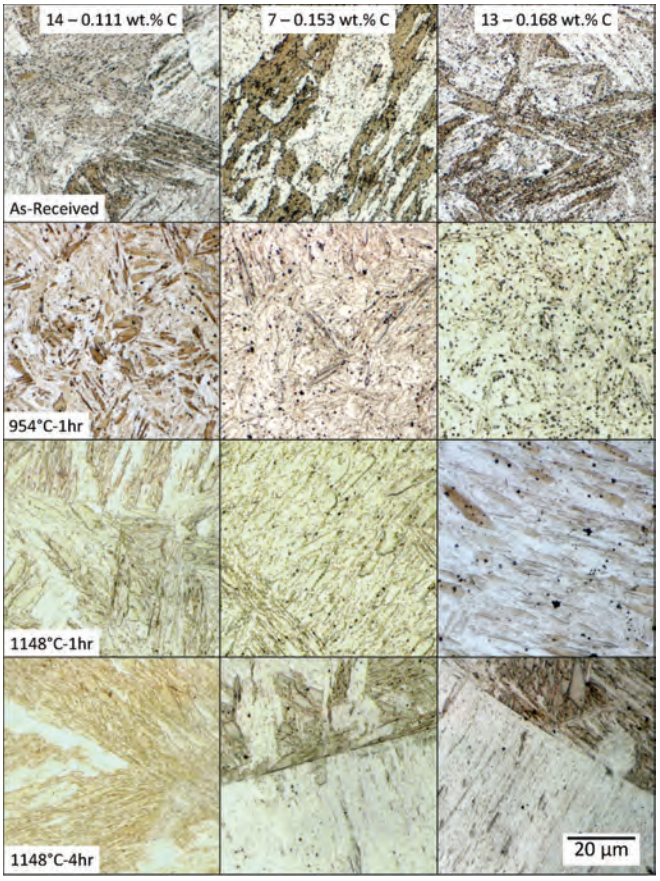

Fig. 4 — Heat 14 (0.111 wt-% C - left), Heat 7 (0.153 wt-% C - middle) and Heat 13 (0.168 wt-% C - right) as-received (top row), after 954°C-1 hour austenization treatment (top middle row), 1148°C-1 hour austenization treatment (bottom middle row), 1148°C-4 hour austenization treatment (bottom row).

rate quenching, the hardness of the as-quenched microstructure is primarily dictated by carbon content. The results of the quenched samples in this study are compared in Fig. 3 to a prediction based on the work of Jaffe and Gordon (Refs. 5, 6).

Each point was based on an average of four separate hardness measurements with a maximum standard deviation for all heats of 0.83 HRC. In the heats with lower carbon content (below 0.14 wt-%), the results align well with the expected value. The hardness of the heats containing more than 0.14 wt-% C is notably lower than the predicted value. One potential explanation for this deviation is that in the experiments conducted by Jaffe and Gordon, the experimental procedure included quenching samples in water followed by cooling in liquid nitrogen. The liquid nitrogen treatment would transform any retained austenite and ensure a 100% martensite structure. (Ref. 7). Although it is possible that there is some fraction of retained austenite in the samples tested in this investigation, it is unlikely that this led to the deviation in hardness shown in Fig. 3. As discussed below, it is more likely the incomplete dissolution of alloy carbides during the austenization process that leads to this discrepancy. The simulated CGHAZ of the four heats indicated by the open symbols in Fig. 3 aligned more closely with the predicted values and exhibited higher, or equal, hardness than the samples from the furnace austenization heat treatments.

Microstructure of the as-quenched and simulated heats. Examination of the microstructure by optical microscopy revealed the primary reason for lower than expected hardness. In several of the heats, particles that are believed to be alloy carbides were present after the solution austenization treatments intended to dissolve them. Figure 4 shows a comparison among three heats representing the range of carbon content studied, Heat 14 (0.111 wt-% C), Heat 7 (0.153 wt-% C), and Heat 13 (0.168 wt-% C) after the 954°C-1 h treatment as well as the microstructure of the materials prior to heat treatment. In all three materials, darker etching particles can be seen with a higher fraction of particles present with increasing carbon content.

Microstructure of Simulated CG-HAZ. For the base metal samples, as the austenization temperature increased, it was expected that the degree of dissolution of alloy carbides would increase. For Heat 14 (0.111 wt-% C), only the sample after the 954°C-1 h treatment had apparent particles present while both of the treatments at 1148°C were free of particles. For the highest carbon Heat 13 (0.168 wt-% C), particles are visible at all three solution austenization treatments with decreasing frequency with increasing temperature and time. Efforts to qualitatively measure the composition of several of these particles were unsuccessful using SEM/EDS

Table 3 — Selected Tempering Treatments

Heat Treatment	Temperature	Time (h)	HJP
HT-1	638°C (1180°F)	1	18215
HT-2	647°C (1197°F)	1.5	18562
HT-3	638°C (1180°F)	6	18924
HT-4	638°C (1180°F)	9	19084
HT-5	677°C (1250°F)	2	19279
HT-6	677°C (1250°F)	5	19657
HT-7	677°C (1250°F)	11	19982

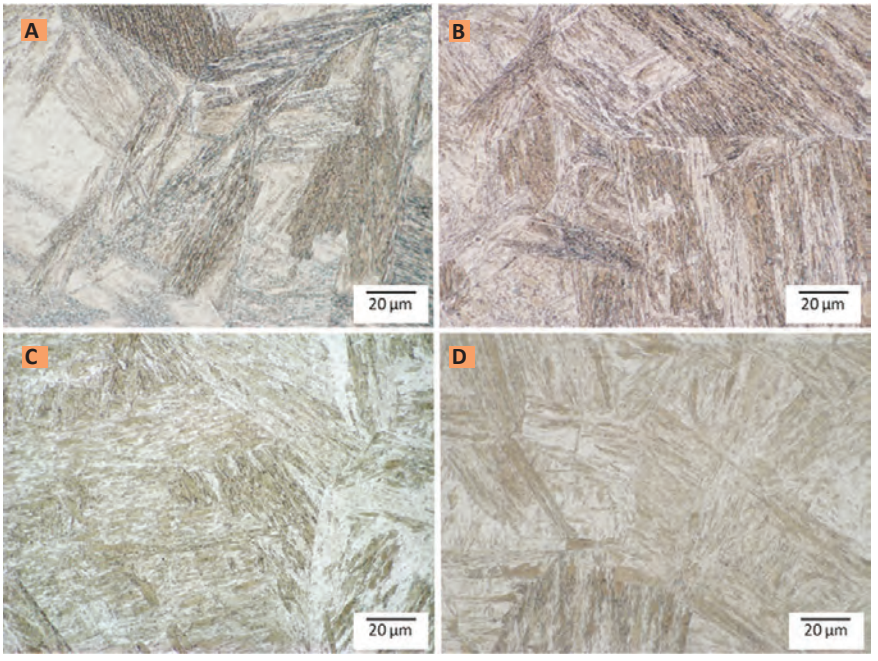

Fig. 5 — Microstructure of the Gleeble simulated CGHAZ: A — Heat 2 (0.108 wt-% C); B — Heat 10 (0.119 wt-% C); C — Heat 5 (0.153 wt-% C); D — Heat 13 (0.168 wt-% C).

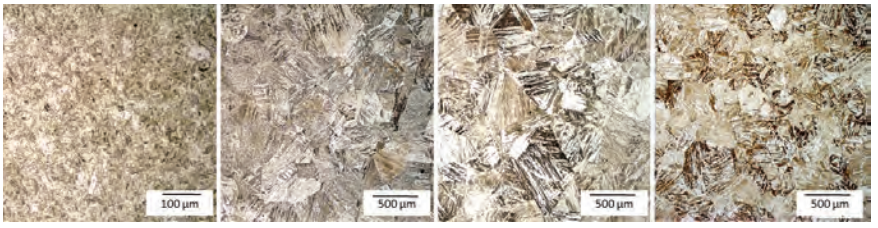

Fig. 6 — Austenite grain growth resulting from 954°C-1 h (left), 1148°C-1 h (middle left) and 1148°C-4 h (middle right) austenization heat treatment of Heat 7 (0.153 wt-% C) and Gleeble HAZ simulation of Heat 5 (0.153 wt-% C) with a 10-s hold time at peak temperature (right).

due to their small size. One possibility is that these particles are the result of precipitation during cooling from the austenization temperature, but carbides forming via this mechanism are typically considerably smaller (Ref. 8). Due to the high cooling rate associated with the water quench and the large size of the particles observed it is likely that they remained through the solution austenization treatments, i.e., their dissolution was incomplete. If these particles are in fact carbides, the result of only partial dissolution would be less carbon available in the austenite at elevated temperature, which would reduce the hardness of the martensite that forms during quenching.

The CGHAZ generated using the Gleeble also resulted in an effectively quenched microstructure, even though cooling occurred in the Gleeble jaws. The high hardenability of F22 ensures that a fully martensitic structure should form under the imposed cooling conditions. The microstructures resulting from these simulations for heats exhibiting a range of carbon contents are shown in Fig. 5. No particles were visible under optical microscopy, indicating that the higher temperature (1350°C) imposed during the simulation was sufficient to dissolve the larger carbides, even at the much shorter times of 1 and 10 s.

An additional indicator of the ineffectiveness of the lower austenization temperatures for solutionizing the preexisting microstructure is the lack of significant grain growth. There was no significant change in the prior austenite grain size for any of the 954°C-1 h austenization heat treatments, even in lower carbon heats such as Heat 14. In the two higher temperature treatments, austenite grain growth became more prevalent as demonstrated by the micrographs of Heat 7 in Fig. 6. In the 1148°C-4 h treatment, the growth is extreme, resulting in prior austenite grain sizes of approximately 310 microns compared to the approximately 40-micron prior austenite grain size of the base material in the as-received condition. This illustrates that while the selected solution austenization treatments were not effective in completely dissolving all precipitates, the two higher temperature treatments did solutionize a high enough fraction to allow for significant grain growth. Despite the higher peak temperature in the CGHAZ simulation, grain growth was less than that in both of the 1148°C furnace treatments with the prior austenite grain size of the 10-s peak temperature hold time of 220 microns. Even without any visible precipitates present, there is not sufficient time at elevated temperature to promote as much grain growth, although the smaller starting prior austenite grain size in Heat 5 of approximately 10 microns may have had an effect on the difference in final grain size when compared to the furnace heat treatments.

Hardness of as-welded heats. As with the simulated CGHAZ, the rapid thermal cycle of the autogenous spot weld is expected to result in a quenched, fully martensitic microstructure within the HAZ. Compared to the furnace heat treatments, the average hardness of the HAZ and the fusion zone of the spot welds are harder in every heat tested in this study. Additionally, the HAZs of the actual welded samples were harder than the simulated CGHAZ in all four heats that were simulated. Not only did the spot welds exceed the hardness of the other test methods, but all heats also exceed the prediction of Jaffe and Gordon as shown in Fig. 7 (Ref. 6).

Because the values plotted are a composite of several regions of the HAZ, there are several different mechanisms that have an effect on the measured hardness. Near the fusion boundary in the CGHAZ, the higher peak temperature results in faster and more complete dissolution of the precipitates present, as confirmed by the simulated CGHAZ samples. Lower

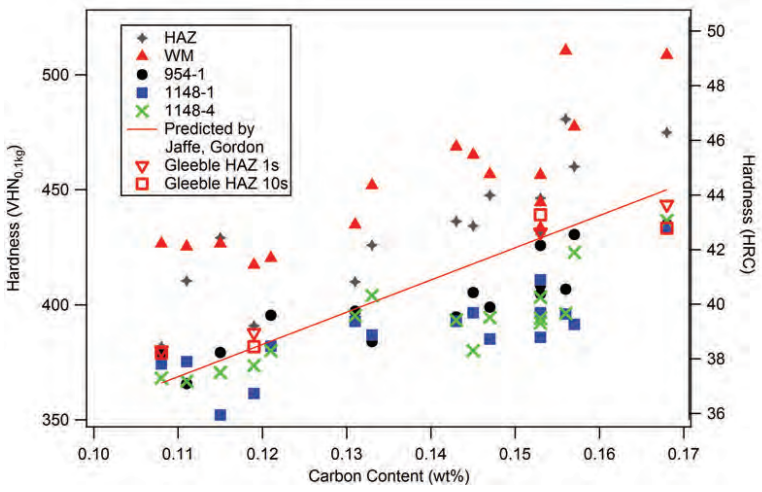

Fig. 7 — Average microhardness of weld heat-affected zone and fusion zone compared to the as-quenched hardness and simulated coarse-grain heat-affected zones (Ref. 6).

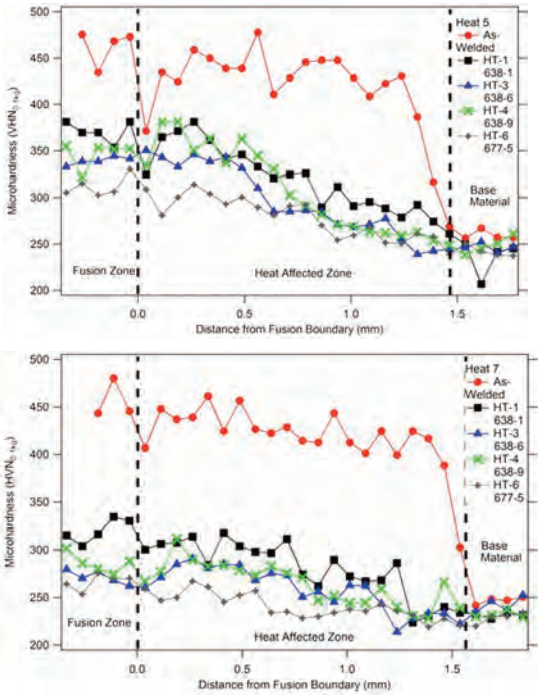

Fig. 8 — Heat 5 (0.153 wt-% C - top) and Heat 7 (0.153 wt-% C - bottom) hardness traverses in the as-welded and tempered condition.

peak temperature farther from the fusion boundary in the fine-grained HAZ (FGHAZ) results in less precipitate dissolution and therefore a lower level of carbon to contribute to transformation strengthening by the formation of martensite (Ref. 9).

The dissolution of the precipitates in the CGHAZ also allows for more grain growth within the CGHAZ. The resulting larger grain size in the coarse-grained region increases the hardenability of the region as well as reduces the contribution to strengthening from a Hall-Petch effect due to the larger martensite block size (Refs. 10–13). The hardness of the fusion zone region of the autogenous spot welds was also measured and exhibited the highest hardness of any of the samples tested. Since this region was completely melted, any precipitates (carbides) would fully dissolve. This would result in the highest possible amount of carbon free to contribute to transformation strengthening.

Hardness of tempered heats. The tempering treatments selected were effective in reducing the hardness of all regions of the autogenous weld samples as shown in Fig. 8 for Heats 5 (0.153 wt-% C) and 7 (0.153 wt-% C). As can be seen, significant reduction in hardness occurs even at the lowest tempering temperature and time (638°C/1 h), which is consistent with Speich who found that the drastic reduction in hardness results from the decomposition of the martensite by the formation of M_3C carbides during the initial stages of tempering (Ref. 8). It is of note that despite similar carbon content and carbon equivalent, Heat 5 (0.153 wt-% C) and Heat 7 (0.153 wt-% C) have different hardness distribution within the HAZ with Heat 5 (0.153 wt-% C) being significantly harder in the coarse-grained region through all of the tempering treatments.

Further tempering resulted in additional softening of the microstructure. Figure 9 shows the reduction of the average hardness of a selection of the autogenous spot welds and simulated CGHAZs. The spot welds shown consist of those with the lowest carbon content (Heat 2 – 0.108 wt-% C), highest carbon content (Heat 13 – 0.168 wt-%), lowest as-tempered hardness (Heat 10 – 0.119 wt-% C), highest tempered hardness (Heat 5 – 0.153 wt-% C) and two additional heats of nearly identical composition (Heats 6 and 7 – 0.153 wt-% C). As expected, the general trend is for the hardness to decrease as the Hollomon-Jaffe parameter is increased. The simulated CGHAZ samples resulted in approximately the same average tempering rate as the spot welds of the same heat for three of the four heats tested. Heat 5 (0.153 wt-% C) had a higher tempered hardness at each Holloman-Jaffe parameter until the values converged during the most severe treatment while Heat 10 (0.119 wt-% C) was noticeably softer earlier in the tempering cycle until the hardness measurements converged during HT-5 and HT-7.

While the general trend for the tempering treatment is lower hardness with a higher Hollomon-Jaffe parameter, there are some heat treatments that result in a secondary hardening effect. This phenomenon is particularly evident in the difference in hardness in the spot weld samples between HT-3 and HT-4, despite both heat treatments being conducted at the same temperature of 638°C. Secondary hardening has been observed in molybdenum containing low-alloy steels and has been attributed to the formation of Mo_2C carbides (Ref. 14). This particular molybdenum-rich carbide can result in an increase in hardness due to the matrix coherency in the early stages of precipitation. Baker and Nutting's investigation into the tempering sequence in 2.25Cr-1Mo steel confirms that in the time and temperature range of both HT-3 and HT-4, Mo_2C-type carbides are present in quenched and tempered martensitic microstructures (Ref. 15) — Fig. 10.

Even when tempering at the highest Hollomon-Jaffe parameter, the as-tempered hardness often did not meet the 22 HRc or 250 VHN hardness requirement set forth by NACE

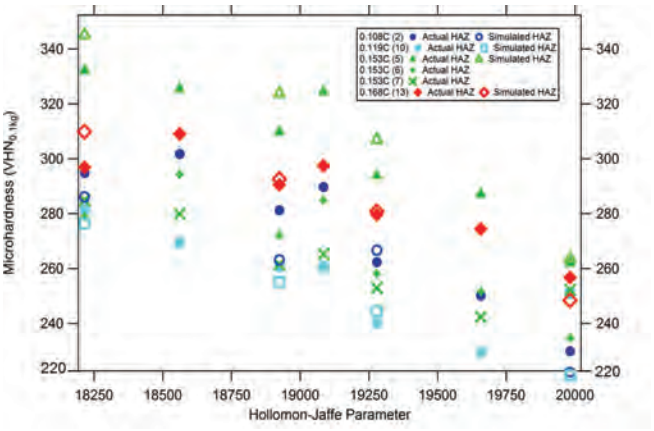

Fig. 9 — Average heat-affected zone and simulated coarse-grain heat-affected zone tempering response.

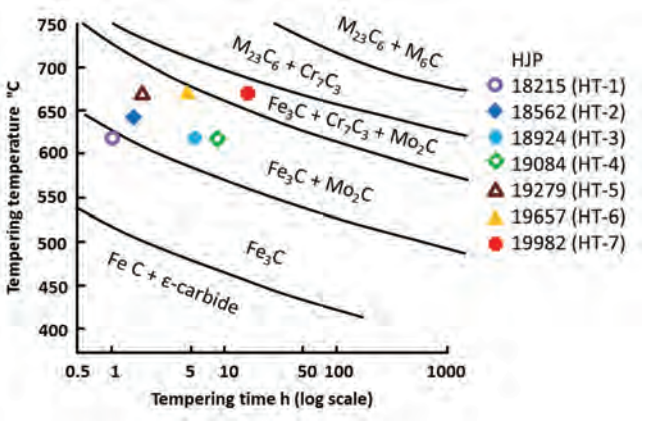

Fig. 10 — Precipitation sequence of F22 in the quenched and tempered condition (Ref. 15). (The Journal of the Iron and Steel Institute).

MR0175. Several factors contribute to the actual industrial postweld heat treatment being more effective than the experiments conducted here. In most cases, the corrosion-resistant cladding is deposited in two passes, which would result in a high-temperature tempering effect of the second pass on the HAZ of the first pass. Additionally, since the target components are typically large, the heating and cooling rates of the actual parts are much slower than those of the small laboratory samples. This will in effect increase the Hollomon-Jaffe parameter, even for the same soak time heat treatment. Since HT-3 is based on a postweld heat treatment cycle commonly used in industrial practice, the secondary hardening effect could be a contributor to difficulty in meeting the maximum hardness requirement by resulting in an unexpected increase in hardness near the end of the tempering treatment.

Conclusions

Solution austenization treatments of 954°C for 1 h, and 1148°C for 1 and 4 h were not sufficient to promote total dissolution of preexisting precipitates in all base material heats and achieve the expected as-quenched hardness. This effect was most pronounced at carbon levels above 0.14 wt-%.

A simulated weld thermal cycle with a peak temperature of 1350°C was effective in dissolving base metal precipitates and achieving predicted as-quenched hardness levels.

The average as-welded hardness of the HAZ and fusion zone exceeded that of the austenitized and quenched base materials.

Most of the heats evaluated in this study did not reach 250 VHN during tempering at 638° and 677°C (1180° and 1250°F) for times up to 11 h.

A secondary hardening reaction resulting from precipitation of Mo_2C opposes the tempering effect predicted by the Holloman-Jaffe parameter.

Acknowledgments

This work was supported by Cameron International (now OneSubsea) through the NSF I/UCRC for Integrated Materials Joining Science for Energy Applications (CIMJSEA). Special thanks to Mr. Dean Hannam from OneSubsea who arranged for the procurement of the F22 materials and provided valuable insight and support throughout the course of the study.

References

1. Berkowitz, B., and Heubaum, F. 1984. The role of hydrogen in sulfide stress cracking of low alloy steels. *Corrosion* 40(5): 240–245.

2. Elboujdaini, M. 2000. Hydrogen-induced cracking and sulfide stress cracking. *Uhlig's Corrosion Handbook*. Wiley.

3. Lippold, J. C., and Fusner, E. 2010. Unpublished research. Columbus, Ohio: The Ohio State University.

4. Hollomon, J., and Jaffe, L. 1945. Time-temperature relations in tempering steel. *Metal Technology* 12: 223–249.

5. Krauss, G. 1999. Martensite in steel: Strength and structure. *Materials Science and Engineering A* 273–275: 40–57.

6. Jaffe, L., and Gordon E. 1957. Temperability of Steels, Transactions. *American Society for Metals* 49: 359–371.

7. Bhadeshia, H. 1983. Carbon content of retained austenite in quenched steels. *Metal Science* 17: 151–152.

8. Speich, G. 1969. Tempering of low-carbon martensite. *Trans Met Soc AIME* 245: 2553–2564.

9. Cottrell, A., and Bilby, B. 1962. Dislocation theory of yielding and strain ageing of iron. *Proc. Phys. Soc. A* 62: 49–62.

10. Doane, D. 1979. Application of hardenability concepts in heat treatment of steel. *Journal of Heat Treating* 1(1): 5–30.

11. Sylwestrowicz, W., and Hall, E. 1951. The deformation and ageing of mild steel. *Proc. Phys. Soc. B* 64(6): 495–502.

12. Petch, N. 1953. The cleavage strength of crystals. *Journal of the Iron and Steel Institue* 173: 25–28.

13. Morito, S., Yoshida, H., Maki, T., and Huang, X. 2006. Effect of block size on the strength of lath martensite in low carbon steels. *Materials Science and Engineering A* 438-440: 237–240.

14. Speich, G. R., and Leslie, W. C. 1972. Tempering of steel. *Metallurgical Transactions* 3(5): 1043–1054.

15. Baker, R., and Nutting, J. 1959. The tempering of 2.25Cr-1Mo steel after quenching and normalizing. *The Journal of the Iron and Steel Institute* 192: 257–268.